Heliyon 7 (2021) e07552

Contents lists available at ScienceDirect

Heliyon

journal homepage: www.cell.com/heliyon

Research article

Differential phosphoprotein signaling in the cortex in mouse models of Gulf War Illness using corticosterone and acetylcholinesterase inhibitors

Julia A. Penatzer [a], Julie V. Miller [b], Nicole Prince [a], Misa Shaw [c,d], Cayla Lynch [c], Mackenzie Newman [c], Gerald R. Hobbs [e], Jonathan W. Boyd [c,*]

[a] C. Eugene Bennett Department of Chemistry, West Virginia University, Morvantown, WV, USA
[b] Cardno ChemRisk, Pittsburgh, PA, USA
[c] Department of Orthopaedics, West Virginia University School of Medicine, Morgantown, WV, USA
[d] Clinical and Translational Science Institute, West Virginia University School of Medicine, Morgantown, WV, USA
[e] Department of Statistics, West Virginia University, Morgantown, WV, USA

ARTICLE INFO

Keywords:
Phosphoprotein signaling
Diisopropyl fluorophosphate
Chlorpyrifos oxon
Corticosterone
Gulf War Illness
Mitogen activated protein kinase

ABSTRACT

Aims: Veterans from the 1990–91 Gulf War were exposed to acetylcholinesterase inhibitors (AChEIs), and, following service, an estimated one-third began suffering from a medically unexplained, multi-symptom illness termed Gulf War Illness (GWI). Previous research has developed validated rodent models that include exposure to exogenous corticosterone (CORT) and AChEIs to simulate high stress and chemical exposures encountered in theater. This combination of exposures in mice resulted in a marked increase in neuroinflammation, which is a common symptom of veterans suffering from GWI. To further elucidate the mechanisms associated with these mouse models of GWI, an investigation into intracellular responses in the cortex were performed to characterize the early cellular signaling changes associated with this exposure-initiated neuroinflammation.

Main methods: Adult male C57BL/6J mice were exposed to CORT in the drinking water (200 μg/mL) for 7 days followed by a single intraperitoneal injection of diisopropyl fluorophosphate (DFP; 4.0 mg/kg) or chlorpyrifos oxon (CPO; 8.0 mg/kg), on day 8 and euthanized 0.5, 2, and 24 h post-injection. Eleven post-translationally modified protein targets were measured using a multiplexed ELISA.

Key findings: Phosphoprotein responses were found to be exposure specific following AChEI insult, with and without CORT. Specifically, CORT + CPO exposure was found to sequentially activate several phosphoproteins involved in mitogen activated protein kinase signaling (p-MEK1/2, p-ERK1/2, and p-JNK). DFP alone similarly increased proteins in this pathway (p-RPS6, and p-JNK), but the addition of CORT ameliorated these affects.

Significance: The results of this study provide insight into differentially activated pathways depending on AChEI in these GWI models.

1. Introduction

Gulf War Illness (GWI) is a chronic, multi-symptom disorder that has afflicted veterans of the 1990–91 Persian Gulf War (GW) since they left theater. Approximately 30% of deployed veterans exhibit a variety of symptoms including cognitive and memory impairments, depression, and gastrointestinal disorders [1, 2, 3, 4, 5, 6, 7]. The symptoms are consistent with features of "sickness behavior," the basis of which is elaboration of inflammatory mediators in the brain, i.e., neuroinflammation [8, 9]. Studies have demonstrated that neuroinflammation is common among GW veterans, and is not confounded by sex, age, or body mass index [10, 11, 12, 13], leading to a consensus that neuroinflammation is a hallmark of GWI [7, 8].

The exact etiology of GWI remains unknown, but the Research Advisory Committee on Gulf War Veterans' Illnesses concluded that exposure to acetylcholinesterase inhibitors (AChEIs) are the most likely cause of the symptoms of GWI [14, 15]; these AChEI exposures include the chemical warfare agent sarin [16], or pesticides, such as chlorpyrifos [17]. Veterans were also exposed to a variety of mental/physical stressors in theater [18]. Therefore, O'Callaghan *et al.* (2015), established a GWI mouse model using corticosterone (CORT; the rodent surrogate for cortisol) pre-treatment at levels that would be associated with high stress in combination with either

* Corresponding author.
E-mail address: Jonathan.boyd@hsc.wvu.edu (J.W. Boyd).

https://doi.org/10.1016/j.heliyon.2021.e07552
Received 1 April 2021; Received in revised form 16 June 2021; Accepted 8 July 2021

diisopropyl fluorophosphate [1] (DFP; sarin surrogate) or chlorpyrifos oxon [2] (CPO; oxon metabolite of chlorpyrifos); these models resulted in marked neuroinflammation characterized as increases in a panel of cytokines and chemokines measured by qPCR. In an effort to elucidate the underlying mechanisms for these observations, Miller *et al.* (2018), measured acetylcholine (ACh) concentrations for each model and found that acetylcholinesterase inhibition is compound specific when pretreated with CORT: CORT ameliorated ACh increase induced by exposure to DFP, but inhibition caused by CPO was not ameliorated by CORT priming [19]. However, both models still resulted in inflammation suggesting an acetylcholinesterase-independent pathway may be the driving force behind the exacerbated neuroinflammation [19].

Cytokine-initiated inflammation, like that observed with these models of neuroinflammation [1, 2], directly initiates cellular signaling changes in impacted tissues, which can be measured through post-translational modifications (PTMs; e.g., protein phosphorylation) at early time points post-exposure [20, 21]. Protein phosphorylation is vital to the coordination of cellular functions and leads to a cascade of cellular signals; however, abnormal or prolonged phosphorylations can lead to dysregulation of signaling pathways, which is the basis of a number of disease states [22, 23, 24, 25, 26]. The family of mitogen-activated protein kinases (MAPKs) are phosphoproteins that are crucial to the intracellular responses to cytokines and have been implicated in neuroinflammatory diseases [27, 28, 29]. Therefore, this study was conducted to identify key phosphorylation events that are involved in these pathways to better elucidate the cellular response mechanisms relevant to these acute exposure models of GWI.

In this study, adult male C57BL/6J mice were exposed to CORT (200 μg/mL) in the drinking water for seven days, and given a single intraperitoneal injection of either DFP (4.0 mg/kg) or CPO (8.0 mg/kg) on the eighth day. Mice were euthanized at 0.5, 2, and 24 h post-exposure, and 11 PTM protein targets were measured in the cortex to understand the temporality of phosphoprotein responses in these validated mouse models of GWI.

2. Results

A panel of phosphoproteins involved in regulatory stress and inflammatory pathways associated with early responses of neuroinflammation were assayed via multiplex bead-based ELISA. The phosphoprotein responses were normalized to controls (saline or peanut oil for DFP and CPO, respectively) in the cortex at 0.5, 2, and 24 h post-exposure.

2.1. Relative phosphorylation responses following DFP exposure

In response to DFP, there were several phosphoproteins that were significantly different ($p < 0.05$) compared to other exposures. RPS6 (S235/S236) was significantly phosphorylated ($p < 0.05$) at 0.5 and 2 h for DFP relative to CORT + DFP and saline, respectively (Figure 1). A significant increase ($p < 0.05$) for p-JNK (T183/Y185) at 24 h post-exposure to DFP alone compared to the other exposures was also

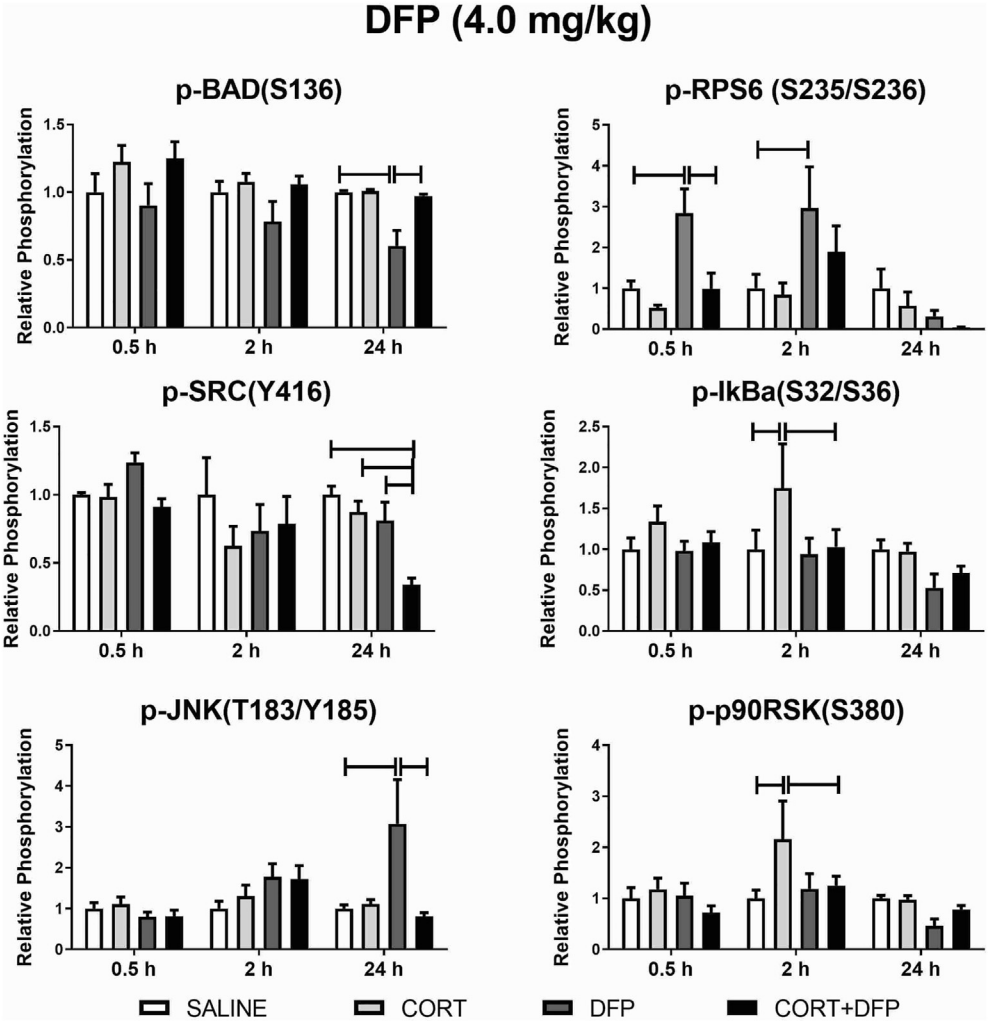

Figure 1. Significant phosphoprotein responses following DFP exposure. Mice were exposed to control or 200 μg/mL CORT in drinking water for 7 days. On day 8, mice were given a single intraperitoneal injection of DFP (4.0 mg/kg) or saline and euthanized via focused microwave irradiation at 0.5, 2, or 24 h post-exposure. Phosphoprotein responses were measured in the cortex using a multiplex ELISA for targets of interest, as described in Materials and Methods. Significance was determined using two-way ANOVA with Bonferroni post-test and a Benjamini and Hochberg test for multiple comparisons, where the horizontal bars represent significance $p < 0.05$ between exposures within a specific time. Data are represented as mean ± SEM with at least $N = 4$ for all phosphoproteins in the figure.

observed (Figure 1). Additionally, DFP resulted in a significant decrease ($p < 0.05$) in p-BAD (S136) at 24 h. At 24 h, there was a significant decrease ($p < 0.05$) for p-SRC (Y416) phosphorylation for CORT + DFP compared to all other exposures (Figure 1). For CORT alone, p-p90RSK (S380) and p-IκBα (S32/S36) were significantly increased ($p < 0.05$) relative to saline and CORT + DFP at 2 h (Figure 1).

Temporally, p-SRC was significantly increased ($p < 0.05$) post-DFP alone at 0.5 h relative to 2 and 24 h (Table 1). There was a significant decrease ($p < 0.05$) in phosphoprotein responses for p-RPS6 and p-CREB (S133) at 24 h post-exposure compared to the early time points (0.5 h and 2 h) after DFP exposure (Table 1). Conversely, p-JNK was significantly increased ($p < 0.05$) at 24 h compared to the early time points for DFP alone. CREB and RPS6 were significantly phosphorylated ($p < 0.05$) at the 2 h time point for CORT + DFP compared to 24 h (Table 1). At 2 h, p-ERK1/2 (T202/Y204, T185/Y187) was also significantly increased ($p < 0.05$) relative to 0.5 and 24 h post-CORT + DFP exposure. SRC phosphorylation was significantly decreased ($p < 0.05$) at 24 h, relative to 0.5 and 2 h, following CORT + DFP exposure. IκBα and p90RSK were also significantly phosphorylated ($p < 0.05$) at the 2 h time point for CORT alone.

2.2. Relative phosphorylation responses following CPO exposure

Unlike DFP alone exposure, CPO alone did not result in any significant differences ($p < 0.05$) from the peanut oil control. Conversely, in response to CORT + CPO, most of the phosphoproteins tested were significantly different ($p < 0.05$) compared to the controls at the specific time points in the cortex (Figure 2). At 2 h, CORT + CPO resulted in significantly ($p < 0.05$) increased phosphorylation of CREB, ERK 1/2, GSK3α/β, IκBα, and MEK 1/2 relative to the controls: peanut oil, CORT, or CPO alone (Figure 2). Conversely, p-BAD (S136), p-ERK 1/2, and p-MEK 1/2 were significantly ($p < 0.05$) decreased at 24 h in response to CORT + CPO exposure relative to the controls (Figure 2). JNK was significantly ($p < 0.05$) phosphorylated at 24 h post-CORT + CPO exposure (Figure 2). For CORT alone, p-ERK1/2 was also significantly increased ($p < 0.05$) at 2 h relative to peanut oil (Figure 2).

Temporally, several of these same phosphoproteins were significantly ($p < 0.05$) increased in response to CORT + CPO or CORT alone at 2 h or 24 h post-exposure (Table 2). CORT + CPO resulted in a significant ($p < 0.05$) increase at 2 h relative to 24 h for p-GSK3α/β. Additionally, p-CREB, p-ERK1/2, and p-MEK1/2 were significantly ($p < 0.05$) increased for CORT + CPO exposure at 2 h relative to 0.5 and 24 h. At 24 h, p-BAD and p-IκBα were significantly ($p < 0.05$) decreased compared to the early time points following CORT + CPO exposure, whereas p-JNK was significantly ($p < 0.05$) increased. CORT alone resulted in a significant ($p < 0.05$) increase at 2 h for p-ERK1/2.

2.3. 3-Way interactions revealed distinct phosphorylation responses

To explore the potential interactions between CORT and AChEIs and how time may affect these interactions, a 3-way interaction was performed on all of the phosphoprotein targets. A 3-way interaction allows us to further determine if the significant effects associated with each target are driven by the different exposures (AChEI or CORT), time, or both. The factors tested were time (0.5, 2, 24 h), and exposure (CORT effect or AChEI effect), and a level of $p < 0.007$ was used to determine significance after a Bonferroni correction. The 3-way interaction revealed p-RPS6, p-CREB, p-ERK1/2, p-IκBα, and p-JNK all were significant for time alone, demonstrating the importance of monitoring the phosphoprotein responses over time (Table 3).

Of the 11 phosphoproteins tested, 6 of the targets (p-BAD, p-RPS6, p-SRC, p-SYK, p-ERK1/2, and p-GSK3α/β) displayed a significant ($p < 0.007$) interaction between CORT, AChEI, or the cross (CORT x AChEI) (Table 3). A significant interaction for CORT represents a difference between the primed with CORT AChEI exposures (CORT + DFP, CORT + CPO) versus those without CORT (DFP, CPO). A significant AChEI interaction differentiates between the AChEI exposures regardless of CORT (CORT + DFP and DFP versus CORT + CPO and CPO). Our

Table 1. Relative phosphoprotein responses following DFP exposure.

Phosphoprotein	Exposure	Time (h)			Significant
		0.5 h	2 h	24 h	
p-RPS6 (S235/S236)	CORT	0.52 ± 0.07	0.85 ± 0.29	0.57 ± 0.34	
	DFP	2.84 ± 0.60	2.96 ± 1.01	0.31 ± 0.15	#,%
	CORT + DFP	0.99 ± 0.38	1.90 ± 0.63	0.04 ± 0.01	%
p-SRC (Y416)	CORT	0.98 ± 0.09	0.63 ± 0.14	0.87 ± 0.08	
	DFP	1.24 ± 0.07	0.73 ± 0.19	0.81 ± 0.13	*,#
	CORT + DFP	0.91 ± 0.06	0.78 ± 0.20	0.34 ± 0.05	#,%
p-CREB (S133)	CORT	1.76 ± 0.64	2.25 ± 0.44	0.83 ± 0.16	
	DFP	1.41 ± 0.62	2.20 ± 1.03	0.16 ± 0.08	%
	CORT + DFP	1.18 ± 0.39	2.67 ± 0.47	0.85 ± 0.21	%
p-ERK1/2 (T202/Y204, T185/Y187)	CORT	1.35 ± 0.27	2.17 ± 0.73	1.06 ± 0.20	
	DFP	0.89 ± 0.24	1.71 ± 0.66	0.94 ± 0.32	
	CORT + DFP	0.66 ± 0.17	2.63 ± 0.87	1.27 ± 0.23	*,%
p-IκBα (S32/S36)	CORT	1.34 ± 0.19	1.75 ± 0.54	0.97 ± 0.10	%
	DFP	0.98 ± 0.12	0.94 ± 0.20	0.53 ± 0.17	
	CORT + DFP	01.08 ± 0.13	1.03 ± 0.21	0.71 ± 0.08	
p-JNK (T183/Y185)	CORT	1.11 ± 0.17	1.30 ± 0.28	1.11 ± 0.11	
	DFP	0.80 ± 0.11	1.78 ± 0.32	3.08 ± 1.09	*,#,%
	CORT + DFP	0.81 ± 0.15	1.72 ± 0.33	0.82 ± 0.09	
p-p90RSK (S380)	CORT	1.18 ± 0.22	2.16 ± 0.75	0.97 ± 0.08	*,%
	DFP	1.06 ± 0.24	1.19 ± 0.30	0.46 ± 0.14	
	CORT + DFP	0.72 ± 0.13	1.25 ± 0.18	0.78 ± 0.08	

Data are represented as mean ± SEM with at least N = 4 for all phosphoproteins. Two-way ANOVA with Bonferroni post-test and the Benjamini and Hochberg test was used for determining significance, where * indicates a significant difference ($p < 0.05$) between 0.5 h vs. 2 h, # indicates a significant difference ($p < 0.05$) between 0.5 h vs. 24 h, and % indicates a significant difference ($p < 0.05$) between 2 h vs. 24 h for a particular exposure.

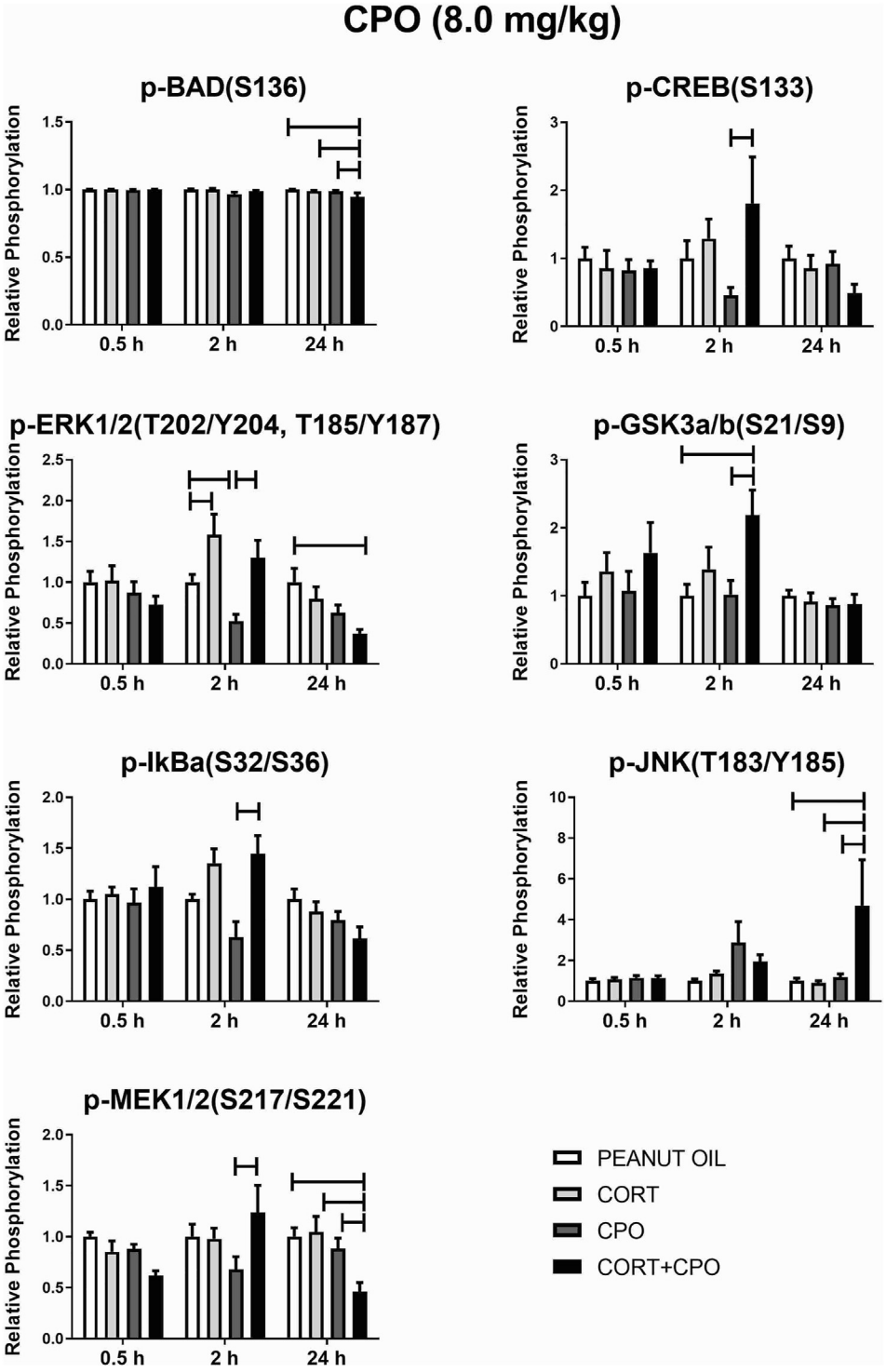

Figure 2. Significant phosphoprotein responses following CPO exposure. Mice were exposed to control or 200 μg/mL of CORT in the drinking water for 7 days. On day 8, mice were given a single intraperitoneal injection of CPO (8.0 mg/kg) or peanut oil and sacrificed via focused microwave irradiation at 0.5, 2, or 24 h post-exposure. Phosphoprotein responses were measured using a multiplex ELISA for targets of interest as described in Materials and Methods. Significance was determined using two-way ANOVA with Bonferroni post-test and a Benjamini and Hochberg test, where the horizontal bars represent significance ($p < 0.05$) between exposures within a specific time. Data are represented as mean ± SEM.

results indicate p-BAD and p-GSK3α/β were significant for the CORT effect demonstrating a significant difference ($p < 0.007$) between the CORT primed exposures (i.e., CORT + DFP and CORT + CPO) from the AChEIs alone (DFP and CPO) (Table 3). The significant CORT interaction provides further evidence of how the mixtures of CORT + AChEIs impact the phosphorylation of specific proteins, and therefore distinguishes from the pathways that are affected by AChEIs alone. Conversely, p-SRC, p-ERK1/2, and p-GSK3α/β were significant ($p < 0.007$) for the AChEI interaction, which indicates these specific phosphoproteins are important to differentiate between the inhibitor exposures regardless of the addition of CORT. A significant cross ($p < 0.007$) between CORT and AChEI was observed for p-BAD, p-RPS6, p-SRC, and p-SYK (Table 3), indicating there was a significant difference between each of the exposures and both interactions attribute to the differences between the four exposures (DFP, CORT + DFP, CPO, CORT + CPO). Thus, these phosphoproteins may be good indicators to differentiate between all the exposures. Additionally, p-JNK and p-SRC demonstrated a significant cross ($p < 0.007$) between all factors (Time

Table 2. Temporal phosphoprotein responses following CPO exposure.

Phosphoprotein	Exposure	Time			Significant
		0.5 h	2 h	24 h	
p-BAD (S136)	CORT	1.00 ± 0.003	1.00 ± 0.01	0.99 ± 0.004	
	CPO	1.00 ± 0.004	0.96 ± 0.02	0.99 ± 0.01	
	CORT + CPO	1.00 ± 0.003	0.99 ± 0.01	0.95 ± 0.03	#,%
p-CREB (S133)	CORT	0.86 ± 0.26	1.29 ± 0.29	0.86 ± 0.19	
	CPO	0.82 ± 0.16	0.45 ± 0.12	0.92 ± 0.18	
	CORT + CPO	0.86 ± 0.11	1.81 ± 0.68	0.49 ± 0.13	*,%
p-ERK1/2 (T202/Y204, T185/Y187)	CORT	1.02 ± 0.18	1.58 ± 0.25	0.80 ± 0.15	*,%
	CPO	0.87 ± 0.14	0.52 ± 0.08	0.63 ± 0.09	
	CORT + CPO	0.73 ± 0.10	1.30 ± 0.22	0.37 ± 0.05	*,%
p-GSK3α/β (S21/S9)	CORT	1.36 ± 0.28	1.39 ± 0.33	0.92 ± 0.13	
	CPO	1.07 ± 0.29	1.02 ± 0.21	0.86 ± 0.09	
	CORT + CPO	1.63 ± 0.44	2.19 ± 0.37	0.88 ± 0.14	%
p-IκBα (S32/S36)	CORT	1.05 ± 0.07	1.35 ± 0.14	0.88 ± 0.10	
	CPO	0.97 ± 0.13	0.63 ± 0.15	0.80 ± 0.08	
	CORT + CPO	1.12 ± 0.20	1.45 ± 0.18	0.62 ± 0.11	#,%
p-JNK (T183/Y185)	CORT	1.07 ± 0.10	1.35 ± 0.13	0.89 ± 0.11	
	CPO	1.16 ± 0.11	2.90 ± 1.01	1.19 ± 0.16	
	CORT + CPO	1.14 ± 0.11	1.95 ± 0.34	4.69 ± 2.24	#,%
p-MEK1/2 (S217/S221)	CORT	0.85 ± 0.11	0.98 ± 0.11	1.05 ± 0.15	
	CPO	0.88 ± 0.05	0.68 ± 0.12	0.88 ± 0.10	
	CORT + CPO	0.62 ± 0.05	1.24 ± 0.27	0.46 ± 0.09	*,%

Data are represented as mean ± SEM. Two-way ANOVA with Bonferroni post-test and a Benjamini and Hochberg test was used for determining significance, where * indicates a significant difference ($p < 0.05$) between 0.5 h vs. 2 h, # indicates a significant difference ($p < 0.05$) between 0.5 h vs. 24 h, and % indicates a significant difference ($p < 0.05$) between 2 h vs. 24 h for a particular exposure.

x CORT x AChEI) (Table 3; Figure 3), displaying that both p-SRC and p-JNK can also differentiate between all the exposures, but in a time dependent manner.

The 3-way interaction analysis provides important insight into how the presence of CORT or AChEI affects the phosphoprotein responses tested. The specific subset of proteins that displayed a significant cross between exposures (p-BAD, p-RPS6, p-SRC, p-SYK, and p-JNK) give us a better understanding of the pathway divergence associated with each exposure and may offer insight into an acetylcholinesterase-independent neuroimmune mechanism of GWI.

Table 3. 3-way interaction revealed distinct phosphoprotein responses.

Phosphoprotein	Interaction	p-value
p-BAD (S136)	CORT x AChEI	0.00007
	CORT	0.00010
	Time	0.00545
p-RPS6 (S235/S236)	Time	0.00066
	CORT x AChEI	0.00498
p-SRC (Y416)	Time x AChEI	0.00001
	CORT x AChEI	0.00021
	AChEI	0.00379
	Time x CORT x AChEI	0.00642
p-SYK (Y352)	CORT x AChEI	0.00247
p-CREB (S133)	Time	0.00058
p-ERK1/2 (T202/Y204, T185/Y187)	Time	0.00000
	AChEI	0.00000
	Time x AChEI	0.00001
	Time x CORT	0.00017
p-GSK3α/β (S21/S9)	AChEI	0.00004
	CORT	0.00117
p-IκBα (S32/S36)	Time	0.00006
p-JNK (T183/Y185)	Time x CORT x AChEI	0.00109
	Time	0.00440

A 3-way interaction was conducted using SAS JMP to determine significant interactions for all 11 phosphoproteins. The factors were time (0.5, 2, 24 h) and exposure (CORT effect or AChEI effect). A significance level of $p < 0.007$ was used to determine statistical significance. Only interactions with statistical significance are shown for each phosphoprotein. A "x" is used to display a cross between two factors.

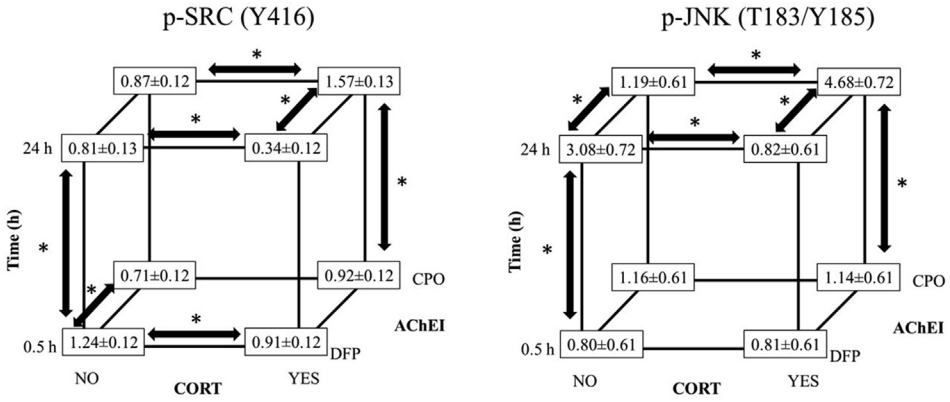

Figure 3. Cube plots for p-SRC (Y416) and p-JNK (T183/Y185). A 3-way interaction was conducted using SAS JMP to determine the main effects and interactions for each phosphoprotein. The factors were time (0.5, 2, 24 h) and exposure (CORT effect or AChEI effect). Cube plots were used to understand the nature of the relationships between the three-factor interactions. The vertices display the fitted mean of the logarithm transformed data ±standard error. Only interactions with a statistically significant 3-way cross are shown ($p < 0.007$), where arrows with * represent the significant differences between the interactions.

2.4. Ingenuity Pathway Analysis (IPA) generated networks

IPA was performed to further explore the pathways and biological processes associated with the tested phosphoprotein responses, while identifying additional nodes of interest for future studies. The normalized phosphorylation responses measured in this study were used to generate a network with a total of 35 nodes, 11 of which are from the dataset, but the remaining 24 are based on connectivity with the dataset and known pathways from literature (Tables 4, 5, and 6) [41]. At 0.5 h, over half of the nodes generated were the same regardless of exposure (Table 4). However, at 2 and 24 h there were only six and four nodes, respectively, that were similar between exposures demonstrating divergence of these networks at later time points (Tables 5 and 6). Specifically, at 2 h post-exposure to DFP alone, 14 of the generated nodes were not found in the other networks (Table 5). At 24 h, the CORT + DFP network generated 20 unique nodes to that exposure (Table 6). Amongst all of the generated networks, two cytokines, tumor necrosis factor (TNF) and interferon gamma (IFN-g), a kinase, PDPK1, and a phosphatase, PTEN, were observed across all of the time points and exposures (Tables 4, 5, and 6). Therefore, these time-independent common nodes are highly connected to the dataset, and may be shared links to the observed neuroinflammation with both of these AChEIs [2, 19, 42].

3. Discussion

A complete understanding of the exposures that led to GWI, as well as viable treatments, have yet to be determined 30 years after the 1990-91 GW. Previous research suggests that exposure to AChEIs, such as sarin or pesticides (e.g., chlorpyrifos), are one of the probable causes of GWI [8, 17, 43]. With this in mind, several rodent models have

Table 4. IPA proposed signaling nodes likely to be involved in the network at 0.5 h.

DFP	CPO	CORT + DFP	CORT + CPO
TNF	TNF	TNF	TNF
PDPK1	PDPK1	PDPK1	PDPK1
IFN-g	IFN-g	IFN-g	IFN-g
PTEN	PTEN	PTEN	PTEN
ALDH1L1	ALDH1L1	ALDH1L1	ALDH1L1
FGR	FGR	FGR	FGR
BTG1	BTG1	BTG1	BTG1
CRK	CRK	CRK	CRK
HAVCR2	HAVCR2	HAVCR2	HAVCR2
RPS6KA3	RPS6KA3	RPS6KA3	RPS6KA3
RASGRF2	RASGRF2	RASGRF2	RASGRF2
ATE1	ATE1	ATE1	ATE1
GPR19	GPR19	GPR19	GPR19
TRAFD1	TRAFD1	TRAFD1	TRAFD1
PPP2R1A	PPP2R1A	PPP2R1A	PPP2R1A
ARID5A	**NCF4**	**CARD6**	**CARD6**
CLEC6A	**ARID5A**	**SH2D2A**	**LRBA**
HCK	**CARD6**	**TOLLIP**	**NCF4**
NKX3-1	**HCK**	**PLCB3**	**PIK3R2**
CNR2	**MAP3K2**	**MAP3K2**	**CDH16**
RASGRF1	**SH2D2A**	**NKX3-1**	**CLEC6A**
LAT2	**TOLLIP**	**UBE2N**	**NKX3-1**
NCF4	**CLEC6A**	**HCK**	**CNR2**
PIK3R2	**LAT2**	**OTUD7B**	**IQGAP1**

IPA networks were generated from the experimental dataset and the top molecules in these pathways were reported. The bolded text represent nodes that were found to be different in at least one exposure, while the normal text represent the nodes that were similar across all exposures. The network p-score (negative log10 (p-value of Fisher's exact test)) for all networks was 28.

Table 5. IPA proposed signaling nodes likely to be involved in the network at 2 h.

DFP	CPO	CORT + DFP	CORT + CPO
TNF	TNF	TNF	TNF
PDPK1	PDPK1	PDPK1	PDPK1
IFN-g	IFN-g	IFN-g	IFN-g
PTEN	PTEN	PTEN	PTEN
ALDH1L1	ALDH1L1	ALDH1L1	ALDH1L1
FGR	FGR	FGR	FGR
CD79B	**CLEC6A**	**ADCY5**	**AKT3**
FCER1G	**GPR19**	**BTG1**	**BTG1**
LAT2	**IKBIP**	**HCK**	**CRK**
PLG	**MAP3K4**	**RASGRF2**	**OTUD78**
ARID5A	**NQO2**	**RPS6KA4**	**RPS6KA3**
CEACAM1	**RASGRF2**	**GPR19**	**TOLLIP**
FCGR2A	**SH2D2A**	**PLCB3**	**CARD6**
LTB4R	**TOLLIP**	**SH2D2A**	**NCF4**
NCF4	**ATE1**	**TNFRSF18**	**RASGRF2**
SELL	**LAT2**	**ATE1**	**TRAFD1**
TREM2	**TRAFD1**	**CRK**	**ATE1**
CLEC6A	**CRK**	**PPP2R1A**	**CLEC6A**
FCGR2B	**HCK**	**TRAFD1**	**GPR19**
HCK	**PLCB3**	**EGR4**	**MAP3K2**
RASGRF1	**UBE2N**	**HAVCR2**	**PLCB3**
TYROBP	**CARD6**	**MAP3K2**	**UBE2N**
CD74	**MAP3K2**	**NFKBID**	**NKX3-1**
FGL2	**RPS6KA3**	**RPS6KA3**	**PPP2R1A**

IPA networks were generated from the experimental dataset and the top molecules in these pathways were reported. The bolded text represent nodes that were found to be different in at least one exposure, while the normal text represent the nodes that were similar across all exposures. The network p-score (negative log10 (p-value of Fisher's exact test)) for all networks was 28.

investigated the role of AChEI exposure, specifically DFP or CPO, in GWI, and related this to significant neurological effects [44, 45, 46, 47, 48, 49]. To build upon the likely exposure to high stress, and better replicate in-theater conditions, rodent models have included exogenous CORT priming in combination with these AChEIs [1, 2, 19]. Studies utilizing these rodent models of GWI have demonstrated exacerbated neuroinflammation in CORT pretreated animals compared to the controls, which has been related to the sickness behavior observed in veterans from the GW [1, 2]. Conversely, Miller *et al.* (2018), displayed differences in acetylcholinesterase inhibition depending on the AChEI (CORT ameliorated ACh increase caused by DFP, but ACh inhibition caused by CPO was not impacted by CORT) [19]. These results suggest a potential acetylcholinesterase-independent route of GWI-related neuroinflammation. To better understand the neurological responses associated with these mouse models of GWI, this study investigated early intracellular signaling responses via phosphoprotein analysis in the cortex.

Exposure to chemical or physical insults perturb the highly dynamic and integrated signaling pathways that lead to either adaptive stress response or cell death [20, 21, 50]. These responses are primarily coordinated by cellular signal transduction networks following the phosphorylation/dephosphorylation cycle mediated by protein kinases and phosphatases [50, 51, 52]. The organ-level response to various chemical and biological exposures, specifically, early cellular processes that involve post-translational phosphorylation events, can regulate adaptive stress and inflammatory pathways that are dependent on both space and time to initiate the appropriate cell signaling cascades [21].

The MAPK signaling pathway is commonly stimulated by a plethora of stress conditions and inflammatory cytokines, resulting in a cascade of phosphorylation and other signaling events that initiate changes for the appropriate biological response (cellular adaptation for survival or death) [53, 54]. Many members of the MAPK family of proteins are implicated in a number of neuroinflammatory diseases [55, 56], and previous research has shown that the MAPK signaling pathway is activated by AChEIs [56, 57], which drives the neuroinflammatory effects of AChEI exposure. Two of the main families of MAPKs were measured in this study: extracellular signal-regulated kinases (ERKs) and c-Jun N-terminal kinases (JNKs).

Our results indicated, CORT + CPO led to significant increases ($p < 0.05$) in phosphorylation of proteins in the MEK/ERK cascade at the early time points (0.5 and 2 h). Specifically, p-MEK1/2, p-ERK1/2, and p-CREB are all significantly increased at 2 h for CORT + CPO relative to the other exposures (Figure 2). This phosphorylation-driven cascade connects signals from cell-surface cytokine receptors (e.g., interleukin-3, granulocyte/macrophage colony stimulating factor) to initiate downstream pathways involved in gene expression [58, 59]. These cytokines trigger the phosphorylation of MEK1/2 and ERK1/2, which ultimately mediates the phosphorylation of RPS6 and CREB [60, 61]. Phosphorylation of RPS6 and CREB has been shown to increase in various brain regions following seizures, but serves a protective role against apoptosis [62, 63, 64].

At 24 h post-exposure to CORT + CPO, a shift in MAPK signaling occurs. Phosphorylated JNK appears to be activated in response to CORT + CPO at the later time point, while p-MEK1/2 and p-ERK1/2 phosphorylation decreases (Figure 2). Moreover, 3-way interaction analysis showed a significant ($p < 0.007$) response for time alone for several proteins involved in MAPK signaling (p-RPS6, p-CREB, p-ERK1/2, and p-JNK; Table 3), further indicating the temporal differences in this pathway. JNKs are typically activated by environmental stressors and inflammatory cytokines (e.g., TNF, IFN-g, interleukin-1), and are well-established to have a central role in activating apoptosis [65, 66, 67, 68]. Locker *et al.* (2017), previously reported significant increases in TNF and interleukin-1 cytokine signaling after CORT + AChEI exposures in these GWI mouse models in the cortex [2]. In this study, IPA analysis also indicated TNF and IFN-g are common nodes between all the exposure networks, independent of time (Tables 4, 5, and 6). All of the temporal responses taken together indicate that early inflammation associated

Table 6. IPA proposed signaling nodes likely to be involved in the network at 24 h.

DFP	CPO	CORT + DFP	CORT + CPO
TNF	TNF	TNF	TNF
PDPK1	PDPK1	PDPK1	PDPK1
IFN-g	IFN-g	IFN-g	IFN-g
PTEN	PTEN	PTEN	PTEN
ARID5A	**ALDH1L1**	**KITLG**	**ALDH1L1**
CEACAM1	**BTG1**	**PIK3CB**	**CLEC6A**
FCGR2A	**CRK**	**ROCK1**	**GPR19**
LTB4R	**RASGRF1**	**TSC1**	**LAT2**
NCF4	**RPS6KA3**	**BRAF**	**NQO2**
CLEC6A	**ARID5A**	**Foxp1**	**RASGRF2**
FCGR2B	**CD79B**	**IL7**	**SH2D2A**
HCK	**FCER1G**	**LRBA**	**ATE1**
RASGRF1	**HCK**	**PIK3CD**	**TRAFD1**
RPS6KA3	**RASGRF2**	**TSC2**	**CRK**
CD74	**SH2D2A**	**CDH16**	**HCK**
FGR	**TOLLIP**	**IQGAP1**	**MAP3K2**
RASGRF2	**ATE1**	**NKX3-1**	**NCF4**
SELL	**CLEC6A**	**PIK3R2**	**PLCB3**
TYROBP	**FGR**	**VHL**	**UBE2N**
CD79B	**PPP2R1A**	**HAVCR2**	**CARD6**
FCER1G	**TRAFD1**	**ITCH**	**FGR**
GPR19	**GPR19**	**S1PR1**	**MAP3K4**
LAT2	**LAT2**	**CNR2**	**RPS6KA3**
PLG	**NCF4**	**TNFSF10**	**TIRAP**

IPA networks were generated from the experimental dataset and the top molecules in these pathways were reported. The bolded text represent nodes that were found to be different in at least one exposure, while the normal text represent the nodes that were similar across all exposures. The network p-score (negative log10 (p-value of Fisher's exact test)) for all networks was 28.

with CORT + CPO involves MAPK proteins that transition from MEK/ERK (pro-survival) to JNK (proapoptotic) in less than 24 h post-exposure. Therefore, p-JNK may serve as a crucial node that links CORT + CPO to prior neuroinflammatory results.

Similar to CORT + CPO, p-JNK is also significantly phosphorylated ($p < 0.05$) at 24 h following DFP alone exposure (Figure 1), but the combination of CORT + DFP ameliorated this significant phosphoprotein response. Therefore, to expand on the differences in phosphoprotein responses to these AChEIs, with and without CORT, we observed significant crosses ($p < 0.007$) from the 3-way interaction. p-BAD, p-RPS6, p-SRC, p-SYK, and p-JNK (Table 3) all displayed a significant cross between CORT and AChEI, indicating that this subset phosphoproteins also play an important role in differentiating between all four exposures (DFP, CPO, CORT + DFP, CORT + CPO). Further, IPA analysis displayed the divergence between all exposure groups, especially at the later time points (2 and 24 h post-exposure; Tables 5 and 6). This was of particular interest because of the commonly observed neuroinflammation, especially for the CORT-primed exposures (CORT + DFP, CORT + CPO), but each exposure leads to disparate cell signaling. These distinctions in phosphoprotein responses, depending on AChEI, may be related to the differences Miller *et al.* (2018) observed in ACh concentrations [19].

The phosphoproteins p-BAD, p-SRC, and p-SYK have crucial relationships that link to the MAPK signaling pathways explored in this study. Growth factors typically induce the phosphorylation of BAD, inactivating its proapoptotic activity [69]. However, p-JNK has been shown to phosphorylate 14-3-3, the sequestering partner of BAD, resulting in an increase in dephosphorylated BAD [70]. Dephosphorylated BAD targets the mitochondria and promotes apoptosis [71]. In the present study, p-BAD is significantly decreased following DFP and CORT + CPO exposures at 24 h (Figures 1 and 2). Meanwhile, the SRC family kinases are highly expressed in the central nervous system and control many cellular events such as cell growth, proliferation, and migration [72]. In this study, the combination of CORT + DFP caused a decrease in p-SRC (Figure 1) that was not observed for DFP alone or the CPO exposures (CPO alone and CORT + CPO). It has been suggested that the decrease in SRC phosphorylation leads to an increase in the degradation and overall loss of N-methyl-D-aspartate receptors following traumatic brain injuries [73, 74]. The loss of N-methyl-D-aspartate receptors has been linked to a number of major nervous system disorders including neurodegenerative diseases, ischemia, pain, and depression [75], which relate to some of the symptoms of GWI. Additionally, SYK, which is involved in multiple biological processes, including adaptive immune response and innate immunity [76, 77], operates together with the SRC family in signaling pathways involved in innate cell response, with SRC being activated first, followed by phosphorylation of SYK [78]. SYK has also been shown to phosphorylate several downstream pathways including the MAPK pathways studied here [79, 80]. Taken together, p-SRC and p-SYK provide interesting biomarkers that link neuroimmune responses to previous findings in these models [1, 2, 19], but their different phosphorylation responses to each AChEI could be used to differentiate between each exposure.

4. Conclusion

Mouse models of GWI were used to explore early cellular signaling changes in the cortex post-exposure to two AChEIs, with and without CORT. These exposures have been shown to cause neuroinflammation [1, 2], but acetylcholinesterase inhibition was AChEI-specific [19]. Here we report a subset of phosphoproteins that are also activated in an AChEI-dependent manner. CORT + CPO appears to be initiating a cell death response via MAPK signaling, indicated by increases in p-JNK, and decreases in p-ERK1/2 and p-MEK1/2. Similarly, DFP activates p-JNK, but CORT priming ameliorates this response; further, our findings indicate that neuroimmune responses to CORT + DFP exposure may be mediated via SRC, which activates a currently unknown independent pathway that may lead to survival, but potentially results in GWI

symptomology. Overall, each exposure (DFP, CPO, CORT + DFP, CORT + CPO) initiates distinct cell signaling cascades. This study found an array of inflammation-activated pathways that may provide insight into the diverse symptomology observed with GWI. Further investigation of the long-term effects of these signal transduction pathways should be conducted to understand the interrelationship of neuroinflammation, acetylcholinesterase inhibition, and phosphoprotein pathways in the disease progression of GWI.

5. Limitations and future directions

As timing is key in many studies, one limitation of these studies was only observing three time points. As indicated by IPA, the nodes in the networks begin to diverge between 0.5 and 2 h. Therefore, future studies must expand on this time course to further understand the progression of the phosphoprotein signaling. Additionally, the present study observed eleven phosphoprotein targets involved in regulatory stress and inflammatory pathways associated with early responses of neuroinflammation; however, based on the present work, an expansion into other downstream targets of SRC and SYK would provide additional information into the differences in these animal models of GWI. Future work will also be completed to provide a global quantitative phosphoproteomics to verify the identified phosphoproteins as well as capture related phosphoproteins not measured in this study at key time points.

6. Materials and Methods

6.1. Materials

The following drugs and chemicals were obtained from the sources indicated: CORT (Steraloids Inc., Newport, RI, USA), CPO (Chem Service, Inc., West Chester, PA, USA), DFP (Sigma-Aldrich Co. St. Louis, MO, USA), ethanol (Sigma-Aldrich), phenylmethylsulfonyl fluoride (Sigma-Aldrich), and cell lysis buffer (Bio-Rad, Hercules, CA, USA). A Pierce BCA assay was obtained from Fisher Scientific (Pittsburgh, PA, USA) and includes albumin standards and working reagent. A custom Bio-Plex Pro multiplexed magnetic bead-based immunoassay kit was purchased from Bio-Rad. The custom kit included capture antibodies, biotinylated secondary antibody, standard diluents, streptavidin-phycoerythrin, resuspension buffer, wash buffer, cell lysis buffer, and positive and negative controls.

6.2. Animals

Adult male C57BL/6J mice (approximately 8–12 weeks of age) were purchased from Jackson Laboratory (Bar Harbor, ME, USA). All procedures were performed under protocols approved by the Institutional Animal Care and Use Committee of the Centers for Disease Control and Prevention, National Institute for Occupational Safety and Health, and the animal facility was certified by the American Association for Accreditation of Laboratory Animal Care. Upon arrival, the mice were individually housed in a temperature- (21 ± 1 °C) and humidity-controlled (50 ± 10%) colony room that was maintained under filtered positive-pressure ventilation on a 12 h light (06:00 h)/12 h dark cycle. The plastic cages were 46 × 25 × 15 cm; cage bedding consisted of heat-treated pine shavings at a depth of 4 cm. Mice were given *ad libitum* access to food and water.

6.3. Dosing

Mice (at least five/group; animals were arbitrarily assigned to groups by the experimenter) were exposed to CORT and AChEIs as previously described [1, 2, 19]. Briefly, mice received CORT in the drinking water (200 μg/mL in 1.2% ethanol) for seven days prior to exposure. Control groups received 1.2% ethanol water. On day eight, mice were given a single intraperitoneal injection of saline (0.9%), peanut oil (CPO vehicle), DFP (4.0 mg/kg), or CPO (8.0 mg/kg) in the morning and returned to their home cage. As with the previously established model, CPO (the oxon metabolite of chlorpyrifos) was used in place of chlorpyrifos to avoid variability related to inter-animal differences in the bioactivation of chlorpyrifos [30, 31, 32].

Preliminary power analyses revealed that an N = 4 was determined to be sufficient for this study to determine phosphoprotein significant differences between exposure groups. In the DFP-exposure cohort: all of the saline (N = 5), CORT alone (N = 5), and CORT + DFP (N = 7) exposed mice survived at the 24 h time point, but only 5 of 14 mice from the DFP exposure alone group survived (36% survival rate). The increased mortality associated with DFP has been noted by several other researchers who have previously used this DFP exposure model [1, 33, 34, 35]. Conversely, for the CPO exposure cohort: all of the peanut oil (N = 5), CORT (N = 5), and CPO (N = 7) exposed mice survived all the time points, but only 5 of 7 mice from the CORT + CPO exposure survived at the 2 h and 24 h time points (71% survival rate).

6.4. Brain dissection

Mice were euthanized at three time points (0.5, 2, and 24 h post-exposure) by focused microwave irradiation. By using focused microwave irradiation for euthanasia, changes to the steady-state levels of protein phosphorylation in response to exposures can be preserved in the brain to provide a snapshot of the early cell signaling alterations that result in long-term impacts using a high-throughput approach [36]. Whole brains were removed from the skull and dissected free-hand with fine curved forceps on a thermoelectric cold plate (Model TCP-2; Aldrich Chemical Co., Milwaukee, WI, USA) to obtain the cortex. Samples were immediately snap frozen and stored at -80 °C until analysis. Mice that did not survive to the end points were excluded from analysis.

6.5. Protein quantification in brain regions

Protein extraction was performed using methods adapted from Hulse *et al.* (2004) [37]. One side of the brain region (e.g., left cortex) was transferred to a 2 mL tube, and 500 μL of cell lysis buffer containing 2 mM phenylmethylsulfonyl fluoride. Samples were homogenized using a sonic dismembrator (model 120; Fisher Scientific) on ice with 3 rapid pulses for 3 s at 35% amplitude until tissue was sufficiently ground (about 5 times). The samples were centrifuged at 4500 x g for 10 min at 4 °C, and the supernatant was collected and stored at -80 °C until analysis. Total protein concentration was determined using the Pierce BCA assay, in duplicate, according to the manufacturer's instructions. Briefly, albumin standards were generated ranging in concentration from 0-2000 μg/mL in sample diluent. Each standard or unknown was pipetted into a microplate well, and 200 μL of the working reagent was added. The plate was incubated at 37 °C for 0.5 h. Absorbance values were determined at 562 nm using an Infinite M1000 plate reader (Tecan, Raleigh, NC, USA).

6.6. Phosphoprotein analysis in discrete brain regions

For phosphoprotein analysis, sample homogenates were diluted to a total protein concentration of 700 μg/mL with sample diluent and centrifuged at 15000 x g for 10 min at 4 °C. Samples were assayed using the Bio-Plex Pro multiplexed magnetic bead-based immunoassay reagent kit for the following targets phosphorylated at the indicated amino acid residues: p-BAD (S136), p-S6 Ribosomal P (S235/S236; p-RPS6), p-SRC (Y416), p-SYK (Y352), p-CREB (S133), p-ERK1/2 (T202/Y204, T185/Y187), p-GSK3α/β (S21/S9), p-IκBα (S32/S36), p-JNK (T183/Y185), p-MEK1/2 (S217/S221), and p-p90RSK (S380). Samples were analyzed using a Bio-Plex 200 suspension array system and Pro II Wash Station (Bio-Rad), according to the manufacturer's instructions. Briefly, the Bio-Plex magnetic bead-based assays follow a typical sandwich ELISA protocol. Capture antibodies are covalently coupled to the beads and react overnight with analytes in the sample. After several washes, a

biotinylated detection antibody is added and incubated for 0.5 h. After another series of washes, the detection complex (streptavidin-phycoerythrin) is added and incubated for 10 min. After a final series of washes, a resuspension buffer is added and data are acquired on the Bio-Plex 200. Biological replicates were at least in quintuplicate, and assay measurements were performed in duplicate (technical replicates). Bio-Rad lysate positive (EGF-treated HEK-293, UV-treated HEK-293, H_2O_2-treated Ramos, EGF-treated SK-BR-3, TNF-α-treated HeLa, SRC-transfected NIH3T3, and PDGF-treated NIH3T3) and negative (phosphatase-treated HeLa) controls were used to ensure appropriate bead counts.

6.7. Statistical analysis

Relative phosphorylation was determined for each target. The averaged raw values were blank-subtracted, and any phosphoprotein non-detects (response was less than blank) were removed before analysis. The blank-subtracted values were then normalized to the respective controls (saline for DFP, peanut oil for CPO) at each time point. A Grubbs' test was performed to remove any significant outliers ($\alpha = 0.05$). As previously mentioned, any non-surviving animals were also excluded from analysis. Thus, these analyses resulted in at least $N = 4$ animals for all phosphoproteins. Data analyses were performed using GraphPad Prism (V5; San Diego, CA, USA) or SAS JMP (V14; Cary, NC, USA). The normalized phosphorylation ± the standard error of the mean (SEM) for each exposure and time point were used to identify significant targets. Two-way analysis of variance (ANOVA) with Bonferroni post-test was used to determine significance using GraphPad Prism. A Benjamini and Hochberg test was performed to correct for multiple comparisons by controlling the false discovery rate. A significance level of 5 % ($p < 0.05$) was considered statistically significant.

A 3-way interaction was then conducted using SAS JMP to determine the main effects and interactions for each phosphoprotein [38]. The factors for the 3-way interaction were time (0.5, 2, 24 h), and exposure (CORT effect or AChEI effect). A threshold of $p < 0.05$ was chosen, and a Bonferroni correction (for the 7 tests) was applied to omit a type I error [39, 40], resulting in a significance level of $p < 0.007$ representing findings that were statistically significant. A 3-way interaction splits the exposures into binary effects of CORT (CORT + DFP and CORT + CPO versus DFP and CPO alone) or AChEI (CPO alone and CORT + CPO versus DFP alone and CORT + DFP), which allows for differences to be easily detected between groups.

6.8. Ingenuity Pathway Analysis (IPA)

The relative phosphorylation responses were further evaluated using QIAGEN's Ingenuity Pathway Analysis (IPA; Redwood City, CA, USA) to understand the network and cellular pathway interactions of the selected phosphoproteins. The proposed networks were generated for all three time points (0.5, 2, and 24 h) following each AChEI exposure with and without CORT (DFP, CPO, CORT + DFP, CORT + CPO). All of the networks were comprised of the experimental dataset in addition to other projected nodes likely to be involved in the network based on the observations from the experimental dataset and Ingenuity's knowledge base. IPA also assigned a p-score (negative $\log_{10}$ (p-value of Fisher's exact test)) to each of the networks. For more information refer to Ingenuity's Analysis (http://pages.ingenuity.com/rs/ingenuity/images/0812%20upstream_regulator_analysis_whitepaper.pdf).

Declarations

Author contribution statement

Julia A. Penatzer, Jonathan W. Boyd: Conceived and designed the experiments; Performed the experiments; Analyzed and interpreted the data; Contributed reagents, materials, analysis tools or data; Wrote the paper.

Julie V. Miller: Conceived and designed the experiments; Performed the experiments; Contributed reagents, materials, analysis tools or data; Wrote the paper.

Nicole Prince: Performed the experiments; Wrote the paper.

Misa Shaw, Cayla Lynch, Mackenzie Newman: Analyzed and interpreted the data; Wrote the paper.

Gerald R. Hobbs: Contributed reagents, materials, analysis tools or data; Wrote the paper.

Funding statement

This work was supported by Congressionally Directed Medical Research Programs: Gulf War Illness Research Program Grants (GW170081).

Data availability statement

Data included in article/supplementary material/referenced in article.

Declaration of interests statement

The authors declare no conflict of interest.

Additional information

No additional information is available for this paper.

Acknowledgements

The authors gratefully acknowledge James P. O'Callaghan, Kimberly A. Kelly, Lindsay T. Michalovicz, Brenda K. Billig, Christopher M. Felton, Ali Yilmaz, and Fang Ma for assistance with dosing the mice and dissecting the brains. The authors would also like to thank Suzanne Danley for her editorial suggestions. Opinions, interpretations, conclusions, and recommendations are those of the author and are not necessarily endorsed by the Department of Defense.

References

[1] J.P. O'Callaghan, K.A. Kelly, A.R. Locker, et al., Corticosterone primes the neuroinflammatory response to DFP in mice: potential animal model of Gulf War Illness, J. Neurochem. 133 (5) (2015) 708–721.

[2] A.R. Locker, L.T. Michalovicz, K.A. Kelly, et al., Corticosterone primes the neuroinflammatory response to Gulf War Illness-relevant organophosphates independently of acetylcholinesterase inhibition, J. Neurochem. 142 (3) (2017) 444–455.

[3] R.F. White, L. Steele, J.P. O'Callaghan, et al., Recent research on Gulf War illness and other health problems in veterans of the 1991 Gulf War: effects of toxicant exposures during deployment, Cortex 74 (2016) 449–475.

[4] R.W. Haley, T.L. Kurt, J. Hom, Is there a Gulf War Syndrome? Searching for syndromes by factor analysis of symptoms, JAMA 277 (3) (1997) 215–222.

[5] J.P. O'Callaghan, L.T. Michalovicz, K.A. Kelly, Supporting a neuroimmune basis of gulf war illness, E. Bio. Med. 13 (2016) 5–6.

[6] U.S. Department of Veterans Affairs Public Health, Gulf War Veterans' Medically Unexplained Illnesses, 2017. https://www.publichealth.va.gov/exposures/gulfwar/medically-unexplained-illness.asp. (Accessed 26 February 2018).

[7] Department of Veterans Affairs, Annual Summary of Federally Sponsored Research on Gulf War Veterans' Illnesses for 2015, Washington, D.C, 2015.

[8] L.T. Michalovicz, K.A. Kelly, K. Sullivan, J.P. O'Callaghan, Acetylcholinesterase inhibitor exposures as an initiating factor in the development of Gulf War Illness, a chronic neuroimmune disorder in deployed veterans, Neuropharmacology 171 (2020) 108073.

[9] L. Steele, A. Sastre, M.M. Gerkovich, M.R. Cook, Complex factors in the etiology of Gulf War illness: wartime exposures and risk factors in veteran subgroups, Environ. Health Perspect. 120 (2012) 112–118.

[10] G.J. Johnson, B.C. Slater, L.A. Leis, T.S. Rector, R.R. Bach, Blood biomarkers of chronic inflammation in gulf war illness, PloS One 11 (6) (2016), e0157855.

[11] T. Whistler, M.A. Fletcher, W. Lonergan, X.R. Zeng, J.M. Lin, A. Laperriere, S.D. Vernon, N.G. Klimas, Impaired immune function in gulf war illness, BMC Med. Genom. 2 (2009) 12.

[12] Z. Alshelh, D.S. Albrecht, C. Bergan, et al., In-vivo imaging of neuroinflammation in veterans with Gulf War illness, Brain Behav. Immun. 87 (2020) 498–507.

[13] D.A. Helmer, W.W. Van Doren, D.R. Litke, C.L. Tseng, L. Ho, O. Osinubi, G.M. Pasinetti, Safety, tolerability and efficacy of dietary supplementation with concord grape juice in gulf war veterans with gulf war illness: a phase I/IIA, randomized, double-blind, placebo-controlled trial, Int. J. Environ. Res. Publ. Health 17 (10) (2020) 3546.

[14] J. Research Advisory Committee on Gulf War Veterans' Illnesses, Gulf War Illness and the Health of Gulf War Veterans: Scientific Findings and Recommendations, Washington, D.C, 2008.

[15] A.A. Brimfield, Chapter seven - chemicals of military deployments: revisiting gulf war syndrome in light of new information, Prog. Mol. Biol. Transl. 112 (2012) 209–230.

[16] T.C. Smith, G.C. Gray, J.C. Weir, et al., Gulf War veterans and Iraqi nerve agents at Khamisiyah: postwar hospitalization data revisited, Am. J. Epidemiol. 158 (5) (2003) 457–467.

[17] K. Choi, H. Joo, R.L. Rose, E. Hodgson, Metabolism of chlorpyrifos and chlorpyrifos oxon by human hepatocytes, J. Biochem. Mol. Toxicol. 20 (6) (2006).

[18] R.M. Sapolsky, L.C. Krey, B.S. McEwen, Prolonged glucocorticoid exposure reduces hippocampal neuron number: implications for aging, J. Neurosci. 5 (1985) 1222–1227.

[19] J.V. Miller, R.F. LeBouf, K.A. Kelly, et al., The neuroinflammatory phenotype in a mouse model of gulf war illness is unrelated to brain regional levels of acetylcholine as measured by quantitative HILIC-UPLC-MS/MS, Toxicol. Sci. 165 (2) (2018) 302–313.

[20] A.A. Han, H.N. Currie, M.S. Loos, et al., Spatiotemporal phosphoprotein distribution and associated cytokine response of a traumatic injury, Cytokine 79 (2016) 12–22.

[21] J.W. Boyd, R. Neubig, Cellular Signal Transduction in Toxicology and Pharmacology: Data Collection, Analysis, and Interpretation, John Wiley & Sons, Ltd, Hoboken, 2019.

[22] F. Ardito, M. Giuliani, D. Perrone, G. Troiano, L.L. Muzio, The crucial role of protein phosphorylation in cell signaling and its use as targeted therapy, Int. J. Mol. Med. 40 (2) (2017) 271–280.

[23] A.S. Dhillon, S. Hagan, O. Rath, W. Kolch, MAP kinase signalling pathways, Oncogene 26 (2007) 3279–3290.

[24] P. Cohen, The role of protein phosphorylation in human health and disease, Eur. J. Biochem. 268 (19) (2001) 5001–5010.

[25] T. Takeuchi, T. Abe, Tyrosine phosphorylated proteins in synovial cells of rheumatoid arthritis, Int. Rev. Immunol. 17 (5-6) (1998) 365–381.

[26] J.K. Lee, N.J. Kim, Recent advances in the inhibition of p38 MAPK as a potential strategy for the treatment of alzheimer's disease, Molecules 22 (8) (2017) 1287.

[27] B. Kaminska, A. Gozdz, M. Zawadzka, A. Ellert-Miklaszewska, M. Lipko, MAPK signal transduction underlying brain inflammation and gliosis as therapeutic target, Anat. Rec. (Hoboken) 292 (12) (2009) 1902–1913.

[28] E. Kotelnikova, N.A. Kiani, D. Messinis, et al., MAPK pathway and B cells overactivation in multiple sclerosis revealed by phosphoproteomics and genomic analysis, PNAS 116 (19) (2019) 9671–9676.

[29] D. Bedognetti, J. Roelands, J. Decock, E. Wang, W. Hendrickx, The MAPK hypothesis: immune-regulatory effects of MAPK-pathway genetic dysregulations and implications for breast cancer immunotherapy, Emerg. Top. Life Sci. 1 (5) (2017) 429–445.

[30] T.B. Cole, B.J. Walter, D.M. Shih, et al., Toxicity of chlorpyrifos and chlorpyrifos oxon in a transgenic mouse model of the human paraoxonase (PON1) Q192R polymorphism, Pharmacogenetics Genom. 15 (2005) 589–598.

[31] W. Jiang, E.G. Duysen, H. Hansen, et al., Mice treated with chlorpyrifos or chlorpyrifos oxon have organophosphorylated tubulin in the brain and disrupted microtubule structures, suggesting a role for tubulin in neurotoxicity associated with exposure to organophosphorus agents, Toxicol. Sci. 115 (2010) 183–193.

[32] W. Jiang, E.G. Duysen, O. Lockridge, Mice treated with a nontoxic dose of chlorpyrifos oxon have diethoxyphosphotyrosine labeled proteins in blood up to 4 days post exposure, detected by mass spectrometry, Toxicology 295 (2012) 15–22.

[33] L.S. Deshpande, D.S. Carter, R.E. Blair, R.J. DeLorenzo, Development of a prolonged calcium plateau in hippocampal neurons in rats surviving status epilepticus induced by the organophosphate diisopropylfluorophosphate, Toxicol. Sci. 116 (2) (2010) 623–631.

[34] H.L. Tripathi, W.L. Dewey, Comparison of the effects of diisopropylfluorophosphate, sarin, soman, and tabun on toxicity and brain acetylcholinesterase activity in mice, J. Toxicol. Environ. Health 26 (4) (1987) 437–446.

[35] H. Zhu, J.J. O'Brien, J.P. O'Callaghan, et al., Nerve agent exposure elicits site-specific changes in protein phosphorylation in mouse brain, Brain Res. 1342 (2010) 11–23.

[36] J.P. O'Callaghan, K. Sriram, Focused microwave irradiation of the brain preserves in vivo protein phosphorylation: comparison with other methods of sacrifice and analysis of multiple phosphoproteins, J. Neurosci. Methods 135 (1-2) (2004) 159–168.

[37] R.E. Hulse, P.E. Kunkler, J.P. Fedynyshyn, R.P. Kraig, Optimization of multiplexed bead-based cytokine immunoassays for rat serum and brain tissue, J. Neurosci. Methods 136 (1) (2004) 87–98.

[38] P. Tavakkolkhah, R. Zimmer, R. Kuffner, Detection of network motifs using three-way ANOVA, PloS One 13 (8) (2018), e0201382.

[39] R.A. Armstrong, When to use the Bonferroni correction, Ophthalmic Physiol. Opt. 34 (5) (2014) 502–508.

[40] T.V. Perneger, What's wrong with Bonferroni adjustments, BMJ 316 (7139) (1998) 1236–1238.

[41] Ingenuity Pathway Analysis, IPA Training: Maximizing the Biological Interaction of Gene, Transcript, & Protein Expression Data with IPA, October 2015. https://chhe.research.ncsu.edu/wordpress/wp-content/uploads/2015/10/IPA-Data-Analysis-training-slides-2016_04.pdf.

[42] K.J. Trageser, M. Sebastian-Valverde, S.X. Naughton, G.M. Pasinetti, The innate immune system and inflammatory priming: potential mechanistic factors in mood disorders and gulf war illness, Front. Psychiatr. 11 (2020) 704.

[43] J. Cao, A. Varnell, D. Cooper, Gulf War Syndrome: a role for organophosphate induced plasticity of locus coeruleus neurons, Nat. Prec. (2011).

[44] J.O. Ojo, L. Abdullah, J. Evans, J.M. Reed, H. Montague, M.J. Mullan, F.C. Crawford, Exposure to an organophosphate pesticide, individually or in combination with other Gulf War agents, impairs synaptic integrity and neuronal differentiation, and is accompanied by subtle microvascular injury in a mouse model of Gulf War agent exposure, Neuropathology 34 (2) (2014) 109–127.

[45] C.M. Hernandez, W.D. Beck, S.X. Naughton, I. Poddar, B.L. Adam, N. Yanasak, C. Middleton, A.V. Terry Jr., Repeated exposure to chlorpyrifos leads to prolonged impairments of axonal transport in the living rodent brain, Neurotoxicology 47 (2015) 17–26.

[46] T.J. Nutter, R.D. Johnson, B.Y. Cooper, A delayed chronic pain like condition with decreased Kv channel activity in a rat model of Gulf War Illness pain syndrome, Neurotoxicology 51 (2015) 67–79.

[47] B.Y. Cooper, R.D. Johnson, T.J. Nutter, Exposure to Gulf War Illness chemicals induces functional muscarinic receptor maladaptations in muscle nociceptors, Neurotoxicology 54 (2016) 99–110.

[48] B.Y. Cooper, L.D. Flunker, R.D. Johnson, T.J. Nutter, Behavioral, cellular and molecular maladaptations covary with exposure to pyridostigmine bromide in a rat model of gulf war illness pain, Toxicol. Appl. Pharamcol 352 (2018) 119–131.

[49] L.K. Flunker, T.J. Nutter, R.D. Johnson, B.Y. Cooper, DEET potentiates the development and persistence of anticholinesterase dependent chronic pain signs in a rat model of Gulf War Illness pain, Toxicol. Appl. Pharmacol. 316 (2017) 48–62.

[50] J.A. Vrana, H.N. Currie, A.A. Han, J. Boyd, Forecasting cell death dose-response from early signal transduction responses in vitro, Toxicol. Sci. 140 (2) (2014) 338–351.

[51] B.N. Kholodenko, Cell-signalling dynamics in time and space, Nat. Rev. Mol. Cell Biol. 7 (3) (2006) 165–176.

[52] R.H. Newman, J. Hu, H.S. Rho, et al., Construction of human activity-based phosphorylation networks, Mol. Syst. Biol. 9 (2013) 655.

[53] D.K. Morrison, MAP kinase pathways, Cold Spring Harb. Perspect. Biol. 4 (11) (2012) a011254.

[54] M. Katz, I. Amit, Y. Yarden, Regulation of MAPKs by growth factors and receptor tyrosine kinases, Biochim. Biophys. Acta 1773 (8) (2009) 1161–1176.

[55] J.E. Lee, J.H. Park, S.J. Jang, H.C. Koh, Rosiglitazone inhibits chlorpyrifos-induced apoptosis via modulation of the oxidative stress and inflammatory response in SH-SY5Y cells, Toxicol. Appl. Pharmacol. 278 (2) (2014) 159–171.

[56] T. Farkhondeh, O. Mehrpour, C. Buhrmann, et al., Organophosphorus compounds and MAPK signaling pathways, Int. J. Mol. Sci. 21 (12) (2020) 4258.

[57] J.A. Te, K.D. Spradling-Reeves, J.F. Dillman, A. Wallqvist, Neuroprotective mechanisms activated in non-seizing rats exposed to sarin, Brain Res. 1618 (2015) 136–148.

[58] C.R. Geest, M. Buitenhuis, M.J. Groot Koerkamp, F.C. Holstege, E. Vellenga, P.J. Coffer, Tight control of MEK-ERK activation is essential in regulating proliferation, survival, and cytokine production of CD34+-derived neutrophil progenitors, Blood 114 (16) (2009) 3402–3412.

[59] F. Chang, L.S. Steelman, J.T. Lee, et al., Signal transduction mediated by the Ras/Raf/MEK/ERK pathway from cytokine receptors to transcription factors: potential targeting for therapeutic intervention, Leukemia 17 (7) (2003) 1263–1293.

[60] J. Xing, J.M. Kornhauser, Z. Xia, E.A. Thiele, M.E. Greenberg, Nerve growth factor activates extracellular signal-regulated kinase and p38 mitogen-activated protein kinase pathways to stimulate CREB serine 133 phosphorylation, Mol. Cell Biol. 18 (4) (1998) 1946–1955.

[61] L.S. Steelman, W.H. Chappell, S.L. Abrams, et al., Roles of the Raf/MEK/ERK and PI3K/PTEN/Akt/mTOR pathways in controlling growth and sensitivity to therapy-implications for cancer and aging, Aging 3 (3) (2011) 192–222.

[62] A. Biever, E. Valjent, E. Puighermanal, Ribosomal protein S6 phosphorylation in the nervous system: from regulation to function, Front. Mol. Neurosci. 8 (2015) 75.

[63] X. Zhu, D. Dubey, C. Bermudez, B.E. Porter, Suppressing cAMP response element-binding protein transcription shortens the duration of status epilepticus and decreases the number of spontaneous seizures in the pilocarpine model of epilepsy, Epilepsia 56 (12) (2015) 1870–1878.

[64] J.A. McCubrey, L.S. Steelman, W.H. Chappell, et al., Roles of the Raf/MEK/ERK pathway in cell growth, malignant transformation and drug resistance, Biochim. Biophys. Acta 1773 (8) (2007) 1263–1284.

[65] D.N. Dhanasekaran, E.P. Reddy, JNK signaling in apoptosis, Oncogene 27 (48) (2008) 6245–6251.

[66] O. Busquets, M. Ettcheto, A. Cano, et al., Role of c-jun N-terminal kinases (JNKs) in epilepsy and metabolic cognitive impairment, Int. J. Mol. Sci. 21 (1) (2020) 255.

[67] S.J. Kim, T.G. Son, K. Kim, et al., Interferon-gamma promotes differentiation of neural progenitor cells via the JNK pathway, Neurochem. Res. 32 (8) (2007) 1399–1406.

[68] M. Guma, G.S. Firestein, c-Jun N-terminal kinase in inflammation and rheumatic diseases, Open Rheumatol. J. 6 (2012) 220–231.

[69] S.R. Datta, A.M. Ranger, M.Z. Lin, et al., Survival factor-mediated BAD phosphorylation raises the mitochondrial threshold for apoptosis, Dev. Cell 3 (5) (2002) 631–643.

[70] K.L. Pennington, T.Y. Chan, M.P. Torres, J.L. Andersen, The dynamic and stress-adaptive signaling hub of 14-3-3: emerging mechanisms of regulation and context-dependent protein–protein interactions, Oncogene 37 (42) (2018) 5587–5604.

[71] J. Sunayama, F. Tsuruta, N. Masuyama, Y. Gotoh, JNK antagonizes Akt-mediated survival signals by phosphorylating 14-3-3, J. Cell Biol. 170 (2) (2005) 295–304.

[72] S.J. Parsons, J.T. Parsons, Src family kinases, key regulators of signal transduction, Oncogene 23 (2004) 7906–7909.

[73] Y. Park, T. Luo, F. Zhang, et al., Downregulation of Src-kinase and glutamate-receptor phosphorylation after traumatic brain injury, J. Cerebr. Blood Flow Metabol. 33 (10) (2013) 1642–1649.

[74] M.W. Salter, L.V. Kalia, Src kinases: a hub for NMDA receptor regulation, Nat. Rev. Neurosci. 5 (4) (2004) 317–328.
[75] Q. Zhou, M. Sheng, NMDA receptors in nervous system diseases, Neuropharmacology 74 (2013) 69–75.
[76] A. Mocsai, J. Ruland, V.L.J. Tybulewicz, The SYK tyrosine kinase: a crucial player in diverse biological functions, Nat. Rev. Immunol. 10 (6) (2016) 387–402.
[77] R.L. Geahlen, Getting SYK: spleen tyrosine kinase as a therapeutic target, Trends Pharmacol. Sci. 35 (8) (2015) 414–422.
[78] C.A. Lowell, Src-family and syk kinases in activating and inhibitory pathways in innate immune cells: signaling cross talk, Cold Spring Harb. Perspect. Biol. 3 (3) (2011) a002352.
[79] T. Kanie, A. Abe, T. Matsuda, et al., TEL-Syk fusion constitutively activates PI3-K/AKT, MAPK and JAK2-independent STAT5 signal pathways, Leukemia 18 (2004) 548–555.
[80] J. Carnevale, L. Ross, A. Puissant, et al., SYK regulates mTOR signaling in AML, Leukemia 27 (11) (2013) 2118–2128.